

Self-Assembly, Structures, and Photophysical Properties of
4,4'-Bipyrazolate-Linked Metallo-Macrocycles with Dimetal Clips[†]Qing-Fu Sun,[‡] Keith Man-Chung Wong,[§] Li-Xia Liu,[‡] Hai-Ping Huang,[‡] Shu-Yan Yu,^{*,‡}
Vivian Wing-Wah Yam,^{*,§} Yi-Zhi Li,^{||} Yuan-Jiang Pan,[⊥] and Kai-Chao Yu[#]

Laboratory for Self-Assembly Chemistry, Department of Chemistry, Renmin University of China, Beijing 100872, P. R. China, Department of Chemistry, The University of Hong Kong, Pokfulam Road, Hong Kong, P. R. China, State Key Laboratory of Coordination Chemistry, Institute of Coordination Chemistry, Nanjing University, Nanjing 210093, P. R. China, Department of Chemistry, Zhejiang University, Hangzhou 310027, P. R. China, and Department of Chemistry, Huazhong University of Science and Technology, Wuhan 430074, P. R. China

Received July 7, 2007

By employing functional diimine ligands coordinated dipalladium(II,II) or diplatinum(II,II) clips as corners and the coplanar 4,4'-bipyrazolate dianion (L^{2-}) ligand as linker, a series of bipyrazolate-bridged metallo-macrocycles, namely, $[M_8L_4](NO_3)_8$ ($M = Pd(dmbpy)$, **1**; $Pd(bpy)$, **2**; $Pt(bpy)$, **3a**; $Pd(phen)$, **4**; $Pt(phen)$, **5**; $Pd(15-crown-5-phen)$, **6**; $Pd(18-crown-6-phen)$, **8**; $Pd(benzo-24-crown-8-phen)$, **10a**; $Pt(15-crown-5-phen)$, **7a**; $Pt(18-crown-6-phen)$, **9a**; $Pt(benzo-24-crown-8-phen)$, **11a**) and $[M_6L_3](NO_3)_6$ ($M = Pt(bpy)$, **3b**; $Pt(15-crown-5-phen)$, **7b**; $Pt(18-crown-6-phen)$, **9b**; $Pd(benzo-24-crown-8-phen)$, **10b**; $Pt(benzo-24-crown-8-phen)$, **11b**), have been synthesized through a directed self-assembly approach that involves spontaneous deprotonation of the 1*H*-bipyrazolyl ligands in aqueous solution. All these compounds have a crown-shaped cavity that can serve as host to solvent molecules and anions. The structures are characterized by elemental analysis, ¹H and ¹³C NMR, ESI-MS, and in the cases of **1a** (the BF_4^- salt of **1**), **2a** (the BF_4^- salt of **2**), and **3b** by single-crystal X-ray diffraction analysis. Photophysical properties for complexes **1** and **2** are discussed.

Introduction

Since the recognition of the multiple bond in $[Re_2Cl_8]^{2-}$ by F. A. Cotton in 1960s, the chemistry of the dimetal- or multimetal-centered compounds has drawn increasing interest due to their structural diversity, rich physical properties and potential applications in catalysis, biological mimicry, magnetic coupling, electron transfer, functional materials, etc.^{1,2} Recently, the utilization of dimetal units as directional

building blocks and the bidentate ligands as linkers has extended such chemistry toward the emerging field of metallo-supramolecular architecture.^{3–9}

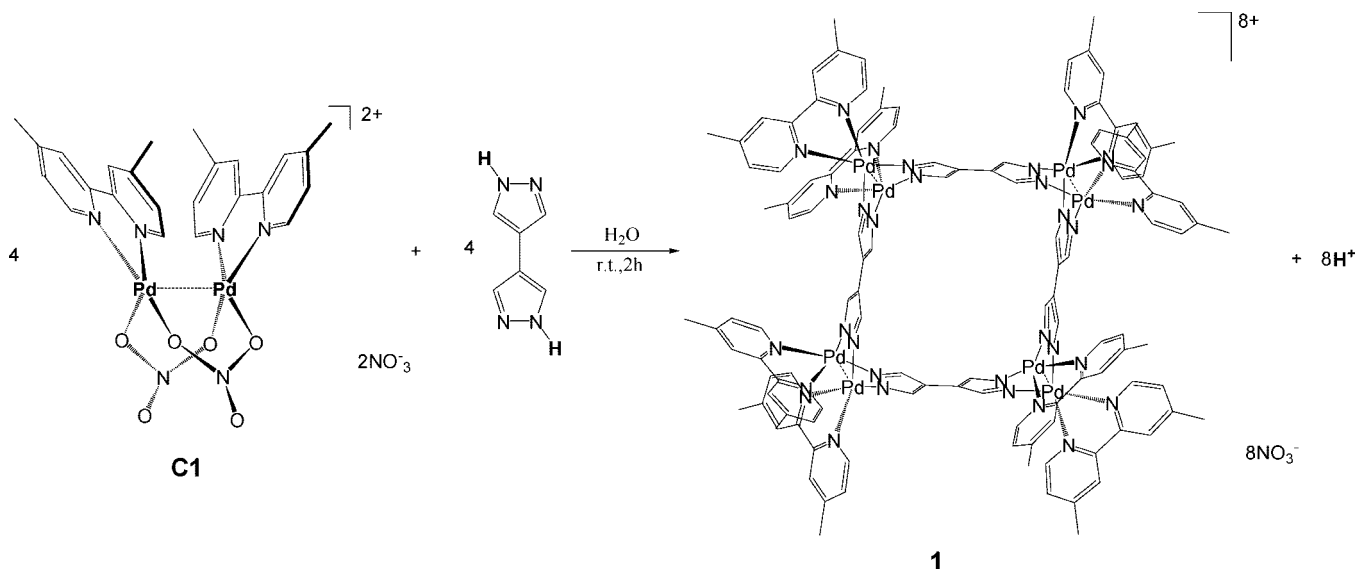
In our search for new coordination motifs with specific functions as building blocks in supramolecular architecture, we noticed that the versatile ligands 1*H*-bipyrazoles could be good alternatives for the widely used carboxylates or other bidentate chelating ligands in binding dimetal centers. Considering the variety of potential applications of pyra-

[†] In memory of Prof. F. Albert Cotton.

* To whom correspondence should be addressed. E-mail: yusy@chem.ruc.edu.cn (S.-Y.Y.), wwyam@hku.hk (V.W.-W.Y.). Fax: +86-10-62516614.

[‡] Renmin University of China.[§] The University of Hong Kong.^{||} Nanjing University.[⊥] Zhejiang University.[#] Huazhong University of Science and Technology.(1) Cotton, F. A.; Murillo, C. A.; Walton, R. A. *Multiple Bonds Between Metal Atoms*, 3rd ed.; Springer Science and Business Media, Inc.: New York, 2005.(2) Chifotides, H.; Dunbar, K. R. *Acc. Chem. Res.* **2005**, *38*, 146.(3) Cotton, F. A.; Lin, C.; Murillo, C. A. *Acc. Chem. Res.* **2001**, *34*, 759.(4) (a) Cotton, F. A.; Lei, P.; Lin, C.; Murillo, C. A.; Wang, X.; Yu, S.-Y.; Zhang, Z.-X. *J. Am. Chem. Soc.* **2004**, *126*, 1518–1525. (b) Cotton, F. A.; Daniels, L. M.; Lin, C.; Murillo, C. A.; Yu, S.-Y. *J. Chem. Soc., Dalton Trans.* **2001**, *121*, 502.(5) Fujita, M.; Tominaga, M.; Hori, A.; Therrien, B. *Acc. Chem. Res.* **2005**, *38*, 371.(6) Leininger, S.; Olenyuk, B.; Stang, P. J. *Chem. Rev.* **2000**, *100*, 853.(7) Dinolfo, P. H.; Hupp, J. T. *Chem. Mater.* **2001**, *13*–3113.(8) Würthner, F.; You, C.-C.; Saha-Möller, C. R. *Chem. Soc. Rev.* **2004**, *33*, 133.(9) Yu, S.-Y.; Zhang, Z.-X.; Cheng, E. C.-C.; Li, Y.-Z.; Yam, V. W.-W.; Huang, H.-P.; Zhang, R. *J. Am. Chem. Soc.* **2005**, *127*, 17994.(10) La Monica, G.; Ardizzoia, G. A.; Karlin, K. D. *Prog. Inorg. Chem.* **1997**, *46*, 151.

Scheme 1



zolate-bridged multimetal coordination compounds,¹⁰ we have started the self-assembly of metallo-macrocycles with bi- or tripyrazolyl ligands.^{11,12}

In our previous article, we reported a new kind of tetramethyl-substituted bipyrazolate linked metallo-macrocycles with dimetal clips [M(bpy)(NO₃)₂]₂(NO₃)₂ or [M(phen)(NO₃)₂]₂(NO₃)₂ (M = Pd or Pt, bpy = 2,2'-bipyridine, phen = 1,10-phenanthroline) through spontaneous deprotonation of the tetramethyl-substituted 1*H*-bipyrazole ligands.¹¹ However, these tetramethyl-substituted bipyrazolate dianion linkers have the interplanar angles of about 50°–90° due to the steric repulsion of the four methyl groups, which result in the distorted metallo-macrocylic structures. In order to obtain highly symmetrical metallo-macrocylic architectures with larger cavities, we expended this kind of self-assembly to the coplanar 4,4'-bipyrazolate ligand.

In the present work, we report the solution self-assembly and structural characterization of a series of metallo-macrocylic complexes with different dipalladium(II,II) or diplatinum(II,II) clips and 4,4'-bipyrazolate dianion linkers. These supramolecular assemblies have been intensively studied by NMR and ESI-MS spectroscopy in solution and in some cases by X-ray crystallographic analysis in solid state. The photophysical properties (electronic absorption and luminescence) of two complexes in solution have also been discussed.

Results and Discussion

Self-Assembly and Characterization of [M₈L₄]⁸⁺-Type Metallo-Macrocycles. The self-assembly of bipyrazolate-bridged metallo-macrocylic complexes **1** is shown in Scheme 1. A mixture of **C1** with the 4,4'-bipyrazole ligand (bpz) in a 1:1 molar ratio in water quantitatively gives the

metallo-macrocylic complexes [Pd₈(dmbpy)₈L₄]·8NO₃ with spontaneous deprotonation of the bpz ligands. The ¹H and ¹³C NMR spectra all indicate the formation of a single product. As shown in ¹H NMR of **1** (Figure 1), 3,3',5,5'-protons of the bpz ligand in the product turn out to be only one singlet at 8.25 ppm, which presents two singlets at 7.87 and 7.70 ppm for H_{3,3} and H_{5,5}, respectively, before self-assembly (see synthesis part). This can only be explained by that the 3,3',5,5'-protons of the bpz in the complex **1** are equivalent. In addition, the protons of the 3,3'-protons of the 4,4'-dimethyl-2,2'-bipyridine (dmbpy) ligand present one singlet at 8.53 ppm in the downfield region of the spectrum (left), and the corresponding resonances of Me groups of the dmbpy ligand appear in the upfield region (right), which also reveal one singlet at 2.70 ppm. All this features can be seen as an indication of a single product with high symmetry.

Moreover, the assignment of product **1** as [M₈L₄]⁸⁺-type macrocycle is further proved by ESI-MS studies, where multiply charged molecular ions corresponding to intact cyclic tetramers were observed. After exchanged into tetrafluoroborate (**1a**), the ESI-MS experiment was performed in acetonitrile solution. As shown in Figure 2, the multiply charged molecular ions of **1a** at *m/z* = 1095.7, 800.1, 622.8, 504.5, 420.0, and 356.7 are ascribed to the cations of [1a - 3BF₄⁻]³⁺, [1a - 4BF₄⁻]⁴⁺, [1a - 5BF₄⁻]⁵⁺, [1a - 6BF₄⁻]⁶⁺, [1a - 7BF₄⁻]⁷⁺, and [1a - 8BF₄⁻]⁸⁺, respectively. Moreover, the multiply charged molecular ions of **1** (nitrate in methanol) at *m/z* = 1054.4, 775.3, 607.8, and 496.3 are assigned to the cations of [1 - 3NO₃⁻]³⁺, [1 - 4NO₃⁻]⁴⁺, [1 - 5NO₃⁻]⁵⁺, and [1 - 6NO₃⁻]⁶⁺, respectively (Figure S17).

In a similar fashion, compound **2** was formed through the combination of dimetal clip **C2** with bpz in the ratio of 1:1. The ¹H and ¹³C NMR spectra confirm the formation of a single product. As shown in Figure 3, the spectra of **2** indicate that a 1:1 complex of **C2** to bpz is formed. The singlet appearing at 8.50 ppm is assigned to the protons of the 3,3',5,5'-protons of the ligand. The ESI-MS experiment of

(11) Yu, S. Y.; Huang, H. P.; Li, S. H.; Jiao, Q.; Li, Y. Z.; Wu, B.; Sei, Y.; Yamaguchi, K.; Pan, Y. J.; Ma, H. W. *Inorg. Chem.* **2005**, *44*, 9471.

(12) Yu, S. Y.; Jiao, Q.; Li, S. H.; Huang, H. P.; Li, Y. Z.; Pan, Y. J.; Sei, Y.; Yamaguchi, K. *Org. Lett.* **2007**, *9*, 1379.

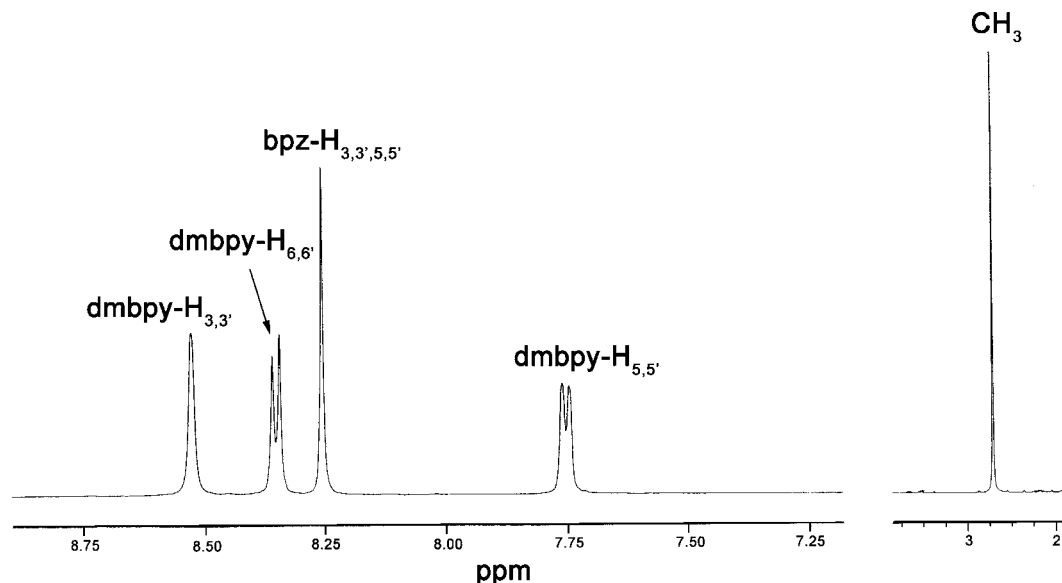


Figure 1. ^1H NMR spectra of **1** in the aromatic region (left, enlarged) and methyl (right) (400 MHz, acetone- d_6 /D $_2$ O = 2:1, 25 °C, TMS).

2 provides strong evidence for the formation of $[\text{Pd}_8(\text{bpy})_8\text{L}_4] \cdot 8\text{NO}_3$ (Figure S18). Multiply charged molecular ions of **2** are observed at $m/z = 979.6, 719.5, 563.7, 459.0, 384.6,$ and 328.4 , corresponding to the cations of $[\mathbf{2} - 3\text{NO}_3^-]^{3+}$, $[\mathbf{2} - 4\text{NO}_3^-]^{4+}$, $[\mathbf{2} - 5\text{NO}_3^-]^{5+}$, $[\mathbf{2} - 6\text{NO}_3^-]^{6+}$, $[\mathbf{2} - 7\text{NO}_3^-]^{7+}$, and $[\mathbf{2} - 8\text{NO}_3^-]^{8+}$, respectively.

As shown in Figure 4, the ^1H NMR spectrum of **4** reveals the formation of 1:1 dimetal clip **C4** to the bpz ligand complex. The singlet at 8.47 ppm is due to protons of the 3,3',5,5'-protons of the ligand, and protons of 5,6-protons of the phenanthroline (phen) ligand shows one singlet at 8.36 ppm. After exchanging into hexafluorophosphate **4a** (Figure S7), the two singlets move to 8.27 and 8.22 ppm, respectively. ESI-MS spectra of **4a** in acetonitrile solution allowed the unambiguous assignment of the $[\text{Pd}_8(\text{phen})_8\text{L}_4] \cdot 8\text{PF}_6$ compositions (Figure 5). For example, multiply charged molecular ions of **4a** at $m/z = 1181.9$ $[\mathbf{4a} - 3\text{PF}_6]^{3+}$, 850.4

$[\mathbf{4a} - 4\text{PF}_6]^{4+}$, 651.0 $[\mathbf{4a} - 5\text{PF}_6]^{5+}$, 581.5 $[\mathbf{4a} - 6\text{PF}_6]^{6+}$, 424.0 $[\mathbf{4a} - 7\text{PF}_6]^{7+}$, and 352.6 $[\mathbf{4a} - 8\text{PF}_6]^{8+}$ were observed. When crown ether fused phenanthroline coordinated dimetal clips **C6** or **C8** are mixed with the bpz ligand in a 1:1 molar ratio in an aqueous solution, bipyrazolate-bridged metallo-macrocyclic complexes $[\text{Pd}_8(15\text{-crown-5-phen})_8\text{L}_4] \cdot 8\text{NO}_3$ (**6**) and $[\text{Pd}_8(18\text{-crown-6-phen})_8\text{L}_4] \cdot 8\text{NO}_3$ (**8**) are formed in quantitative total yield, respectively. The ^1H NMR spectrum of **6** is depicted in Figure 6. The singlet at 8.54 ppm is due to protons of the 3,3',5,5'-protons of the bpz ligand, and protons of methylene due to the crown ether shows four sets of signals at 4.65, 4.21, 3.94, and 3.90 ppm. After exchanging into hexafluorophosphate **6a** (Figure S10), the singlet of the bpz reveals a 0.37 ppm shift to the up-field. The ESI-MS spectra of **6a** in acetonitrile solution allowed the clear assignment of the $[\text{Pd}_8(15\text{-crown-5-phen})_8\text{L}_4] \cdot 8\text{PF}_6$ compositions (Figure S19). For example,

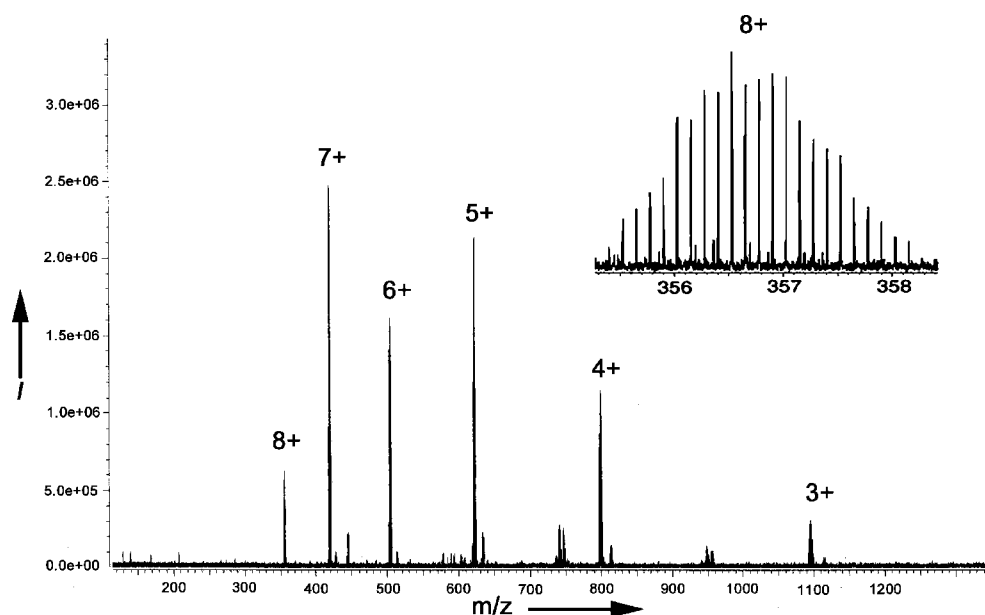


Figure 2. ESI-MS spectra of **1a** in acetonitrile; the inset shows the isotopic distribution of the species $[\mathbf{1} - 8\text{BF}_4^-]^{8+}$.

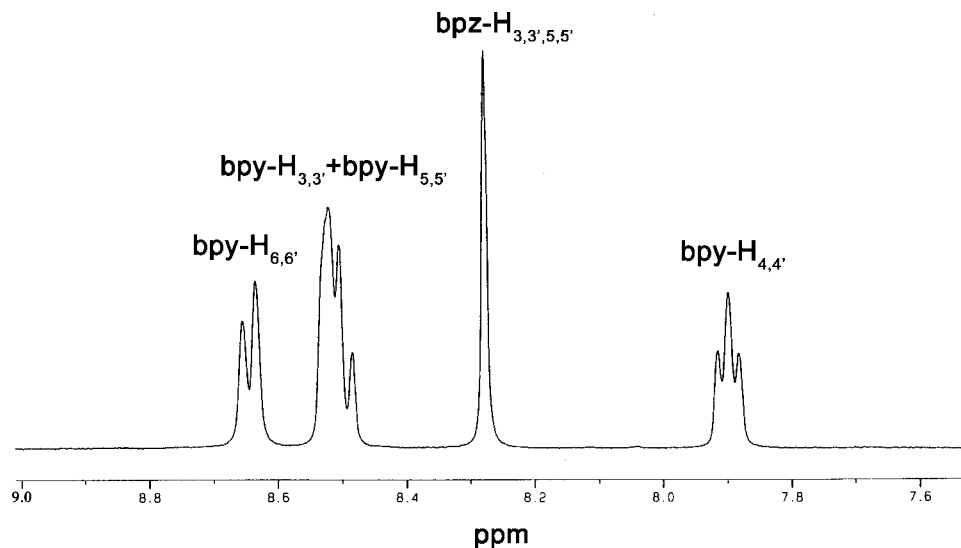


Figure 3. ^1H NMR spectra of **2** (400 MHz, acetone- d_6 /D $_2$ O = 2:1, 25 °C, TMS).

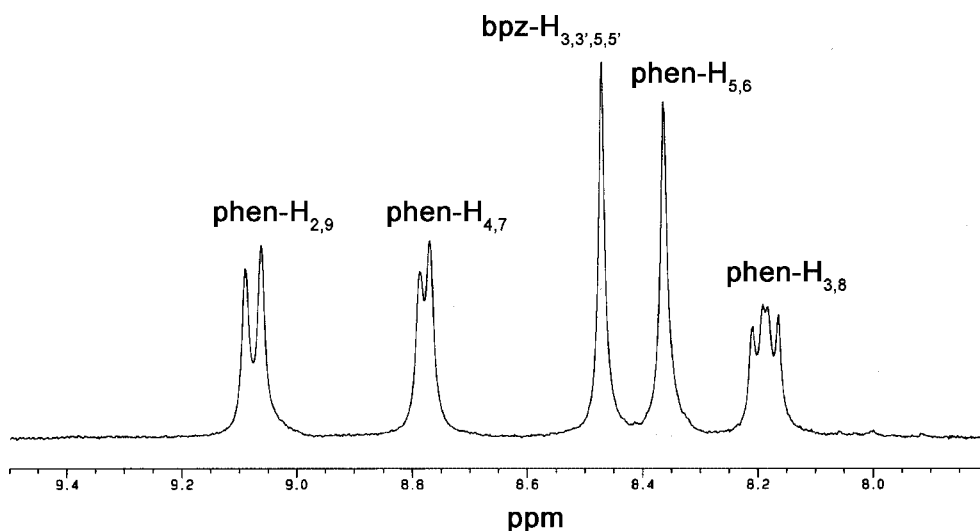


Figure 4. ^1H NMR spectra of **4** (400 MHz, DMSO- d_6 , 25 °C, TMS).

multiply charged molecular ions of **6a** at $m/z = 1689.1$ [**6a** - 3PF_6] $^{3+}$, 1230.6 [**6a** - 4PF_6] $^{4+}$, 955.7 [**6a** - 5PF_6] $^{5+}$, 772.3 [**6a** - 6PF_6] $^{6+}$, and 641.2 [**6a** - 7PF_6] $^{7+}$ were observed.

Self-Assembly and Characterization of $[\text{M}_8\text{L}_4]^{8+}$ and $[\text{M}_6\text{L}_3]^{6+}$ -Type Metallo-Macrocycles. The self-assembly of bipyrazolate-bridged metallo-macrocyclic complexes **3a** and **3b** is shown in Scheme 2. Dimetal clip **C3** mixed with the bpz ligand in a 1:1 molar ratio in water results in the formation of bipyrazolate-linked metallo-macrocyclic complexes $[\text{Pt}_8(\text{bpy})_8\text{L}_4] \cdot 8\text{NO}_3$ and $[\text{Pt}_6(\text{bpy})_6\text{L}_3] \cdot 6\text{NO}_3$ with spontaneous deprotonation from the bpz ligand. The ^1H NMR spectra indicate the formation of two products. The assignments of products **3a** and **3b** as $[\text{Pt}_8\text{L}_4]$ and $[\text{Pt}_6\text{L}_3]$ -type macrocycles are based on ESI-MS studies where multiply charged molecular ions corresponding to intact cyclic trimers and tetramers were observed. Single crystal of **3b** was obtained by the vapor diffusion of diethyl ether into their methanol solutions. The structure of **3b** was determined via X-ray crystallography and revealed the $[\text{M}_6\text{L}_3]^{6+}$ -type macrocycles.

The solution of the 1:1 complex of **C3** to bpz coordination was measured by ^1H NMR spectroscopy (Figure 7) in 2:1

D $_2$ O-acetone- d_6 . Notably, only two singlets are observed in the aromatic region at 8.44 and 8.38 ppm of the spectrum which correspond to the two assemblies (**3a** and **3b**) in the solution with yields of ca. 50 and 50%, respectively. The ESI MS experiments provide strong evidence for the formation of $[\text{Pt}_8(\text{bpy})_8\text{L}_4] \cdot 8\text{NO}_3$ (**3a**) and $[\text{Pt}_6(\text{bpy})_6\text{L}_3] \cdot 6\text{NO}_3$ (**3b**) (Figure 8). In the ESI-MS spectrum of the mixture of **3a** and **3b**, the peaks appearing at $m/z = 896.9$ [**3a** - 4NO_3^-] $^{4+}$ and [**3b** - 3NO_3^-] $^{3+}$, 704.9 [**3a** - 5NO_3^-] $^{5+}$, 656.8 [**3b** - 4NO_3^-] $^{4+}$, 577.1 [**3a** - 6NO_3^-] $^{6+}$, and 513.2 [**3b** - 5NO_3^-] $^{5+}$ were observed.

When dimetal clips **C5**, **C7**, **C9**, **C10**, or **C11** are mixed with the bpz ligand in a 1:1 molar ratio in an aqueous solution, bipyrazolate-bridged metallo-macrocyclic complexes $[\text{Pt}_8(\text{phen})_8\text{L}_4] \cdot 8\text{PF}_6$ (**5a**, 97%), $[\text{Pt}_8(15\text{-crown-5-phen})_8\text{L}_4] \cdot 8\text{NO}_3$ (**7a**, 65%), $[\text{Pt}_6(15\text{-crown-5-phen})_6\text{L}_3] \cdot 6\text{NO}_3$ (**7b**, 24%), $[\text{Pt}_{2n}(15\text{-crown-5-phen})_{2n}\text{L}_n] \cdot 2n\text{NO}_3$ ($n > 4$, **7c**, 11%), $[\text{Pt}_8(18\text{-crown-6-phen})_8\text{L}_4] \cdot 8\text{NO}_3$ (**9a**, 50%), $[\text{Pt}_6(18\text{-crown-6-phen})_6\text{L}_3] \cdot 6\text{NO}_3$ (**9b**, 50%), $[\text{Pd}_8(\text{benzo-24-crown-8-phen})_8\text{L}_4] \cdot 8\text{NO}_3$ (**10a**, 65%), $[\text{Pd}_6(\text{benzo-24-crown-8-phen})_6\text{L}_4] \cdot 6\text{NO}_3$

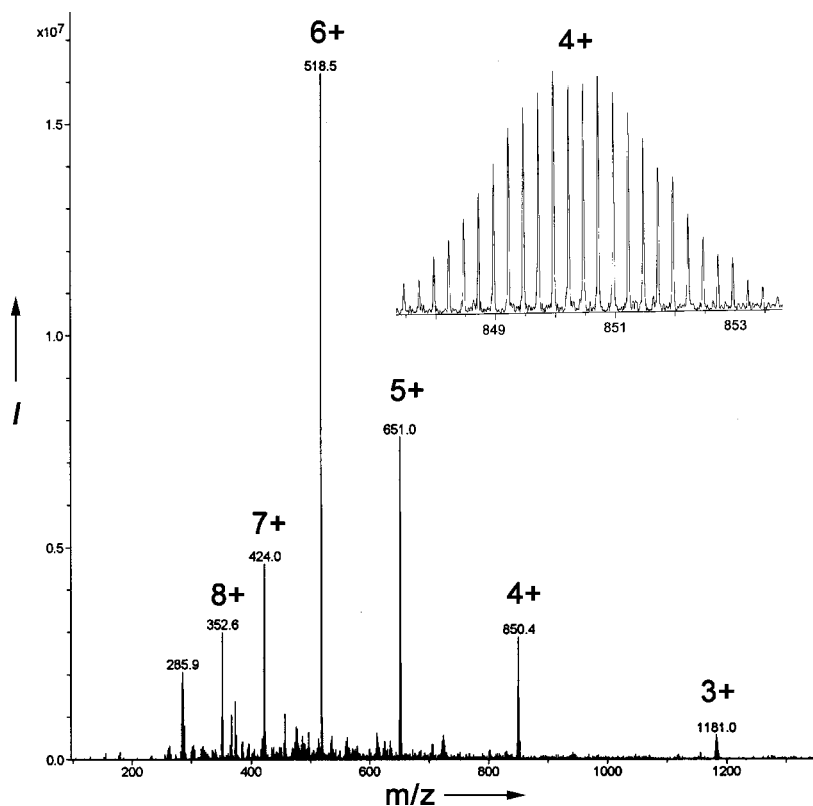


Figure 5. ESI-MS spectra of **4a** in acetonitrile; the inset shows the isotopic distribution of the species $[4 - 4PF_6^-]^{4+}$.

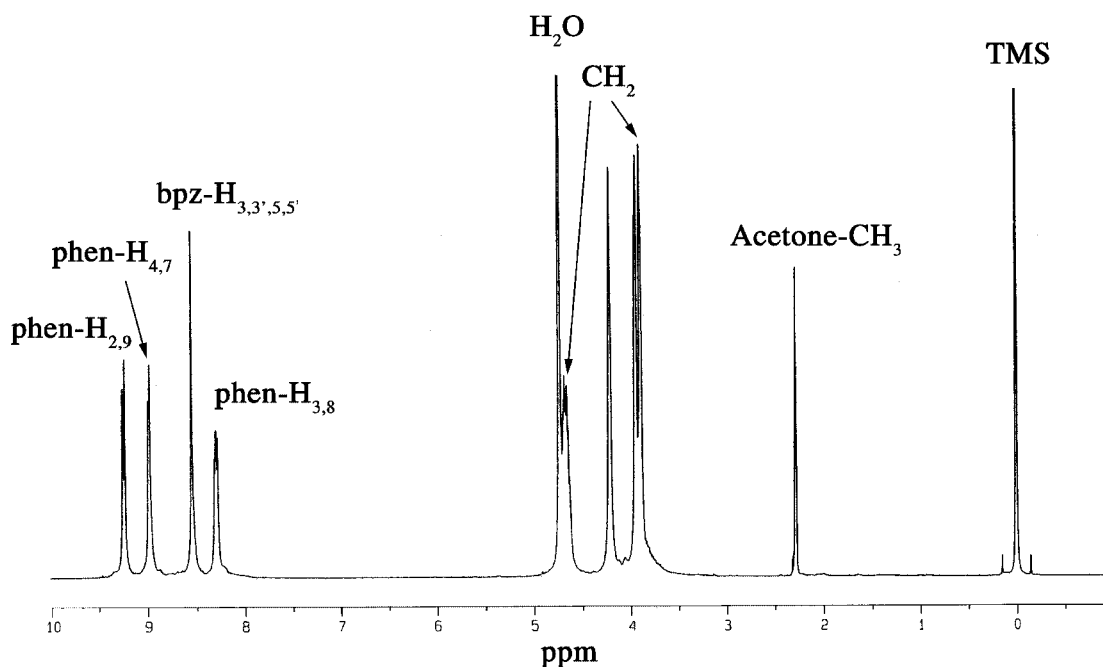


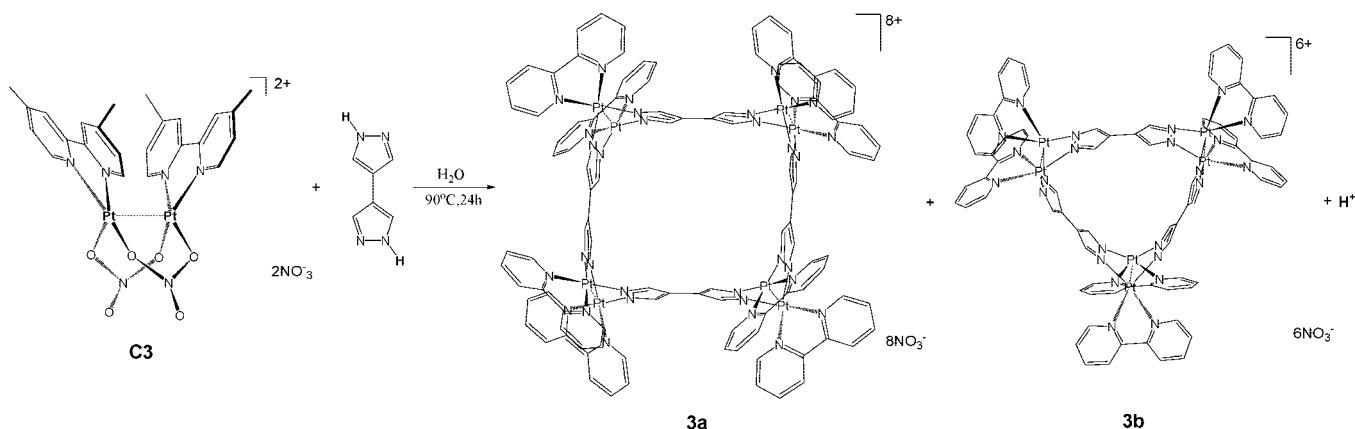
Figure 6. 1H NMR spectra of **6** (400 MHz, acetone- d_6 /D $_2$ O = 2:1, 25 °C, TMS).

(**10b**, 35%), $[Pt_8(\text{benzo-24-crown-8-phen})_8L_4] \cdot 8NO_3$ (**11a**, 85%), and $[Pt_6(\text{benzo-24-crown-8-phen})_6L_4] \cdot 6NO_3$ (**11b**, 15%) are formed in quantitative total yield.

Crystal Structures of the Metallo-Macrocycles. Single crystal of **1a** (the BF_4^- salt of **1**) was obtained by vapor diffusion of diethyl ether into its acetonitrile solutions. An ORTEP representation of **1a** is shown in Figure 9. Selected bond lengths and bond angles are listed in Table S1. The complex **1a** crystallized in the monoclinic space group $C2/$

m. The crystal structure of **1a** also displays a similar tetragonal Pd_8 crown-shaped metallo-macrocyclic structure with four $(\mu\text{-pyrazolato-}N,N')$ doubly bridged $[(\text{dmbpy})Pd]_2$ dimetal corners as that of **2a**. The dihedral angle between the dmbpy ligands within the dimetal corner is 86.4° , and the separation of $Pd1 \cdots Pd2$ is $3.345(1) \text{ \AA}$ displaying weak $Pd \cdots Pd$ interactions, which are all similar to that of **2a**. The dihedral angle between two pyrazolate planes in the dipalladium corner is 88.9° , and the two pyrazolate planes

Scheme 2



in the bpz ligand are almost coplanar with the interplanar angles 1.1° (N7–N8–C28–C29–C30) and 4.6° (N5–N6–C25–C26–C27). These leads to the nearly square metallo-macrocyclic structure with a significantly larger cavity with dimensions of $9.1 \times 9.1 \text{ \AA}$, as defined by the distances between adjacent dipalladium centers. The side view of **2a** presents a crown conformation with a side length of the crown rims $\approx 20 \text{ \AA}$ and a cavity depth $\approx 10.0 \text{ \AA}$. Several water molecules are included inside the cavity. In the crystal, complex **1a** stacks by intermolecular π – π stacking interactions of the dmbpy rings with a contact distance of $3.584(3) \text{ \AA}$ between the neighboring molecules (Figure S21).

An ORTEP representation of **2a** is depicted in Figure 10. Selected bond lengths and bond angles are listed in Table S3. Complex **2a** crystallizes in the triclinic space group $P\bar{1}$ with 14 cocrystallized water molecules. As shown in Figure 10, complex **2a** displays a tetragonal Pd₈ crown-shaped metallo-macrocyclic structure with four (μ -pyrazolato- N,N')₂ doubly bridged [(bpy)Pd]₂ corners. In the dipalladium corners, the dihedral angles, defined by N5–N6–Pd2–Pd1 plane and N7–N7–Pd1–Pd2 plane, or N13–N14–Pd4–Pd3 plane and N15–N16–Pd3–Pd4 plane, are 107.6° and 100.0° , respectively. There are no π – π stacking interaction between the (bpy)Pd planes within each corner because of large dihedral angles (106.8° and 67.6°). The separations of

Pd1Pd2 ($3.434(1) \text{ \AA}$) and Pd3...Pd4 ($3.221(1) \text{ \AA}$) are near the sum of the van der Waals radii of palladium (the typical value 1.6 \AA), which reveal quite weak Pd...Pd interactions. While the dihedral angles between two pyrazolate planes in the dipalladium corners are 92.3° (Pd1Pd2 corner) and 95.5° (Pd3Pd4 corner), the two pyrazolate planes in the bpz ligand are almost coplanar with dihedral angles about 10° . These leads to the nearly square metallo-macrocyclic structure with a significantly larger cavity with dimensions of $9.0 \times 9.0 \text{ \AA}$, defined by the distances between adjacent dipalladium centers. The side view of **2a** also presents a crown conformation with a side length of the crown rims $\approx 16 \text{ \AA}$ and a cavity depth $\approx 10.0 \text{ \AA}$. The most fascinating feature of the structure is the binding of two BF₄⁻ anions into the cavity by electrostatic interaction between Pd1 and F15 with the separation of 3.113 \AA (F15...Pd1). Other BF₄⁻ anions are located near the cation by weak C–H...F interactions as list in Table S3. In the crystal, complex **2a** stacks by weak intermolecular π ... π stacking interactions with a contact distance of $3.672(3) \text{ \AA}$ between the bpy rings of neighboring molecules (Figure S22).

As shown in Figure 11, compound **3b** also displays a crown-shaped trigonal Pt₆ macrocyclic structure with three (μ -pyrazolato- N,N')₂ doubly bridged [(bpy)Pt]₂ corners. The midpoints of the three diplatium corners define a triangle

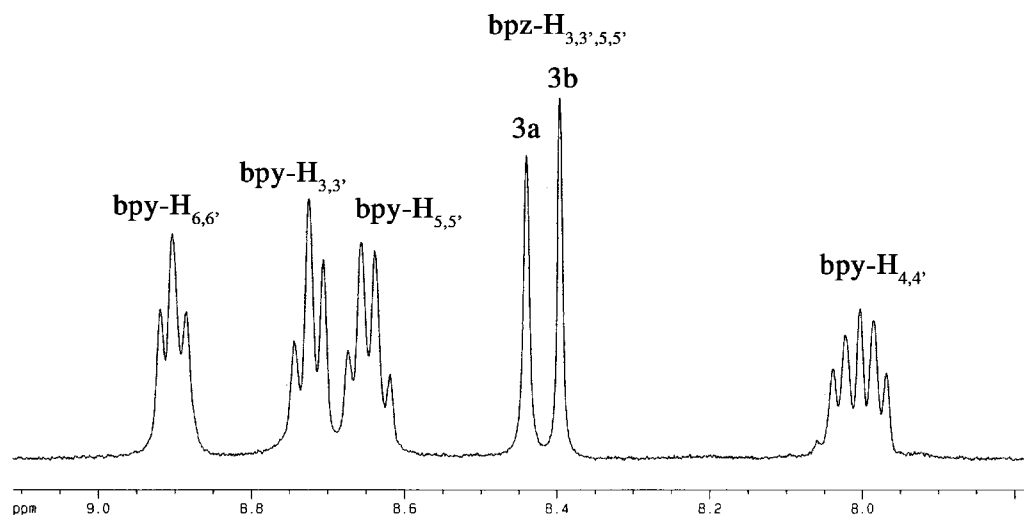


Figure 7. ¹H NMR spectra of **3a** and **3b** (400 MHz, acetone-*d*₆/D₂O = 2:1, 25 °C, TMS).

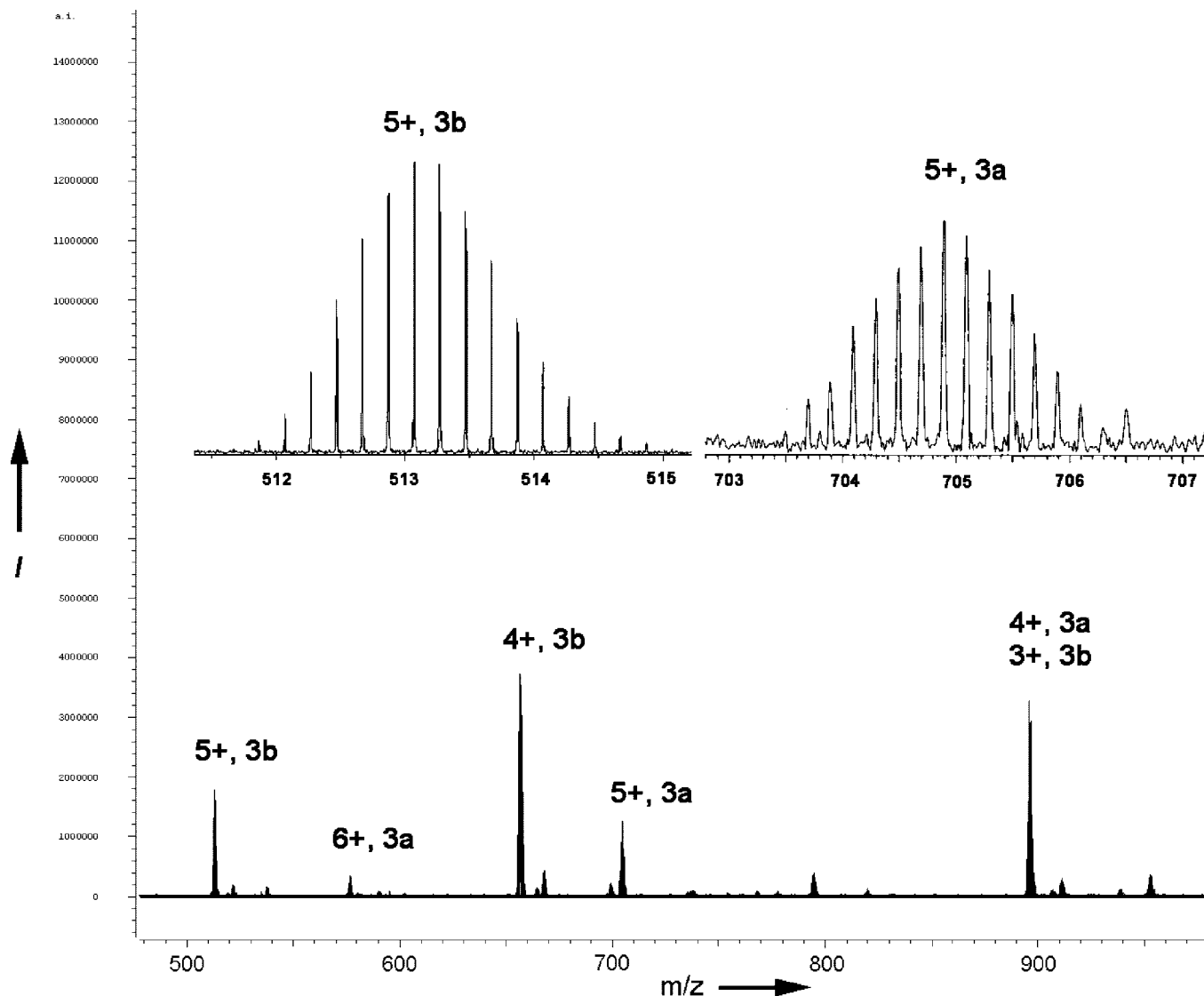


Figure 8. ESI-MS spectra of **3a** and **3b** in methanol; the inset shows the isotopic distribution of the species $[3a - 5NO_3^-]^{5+}$ and $[3b - 5NO_3^-]^{5+}$.

with an average side length of 9.0 Å. The two internal angles of the triangle, defined by N9–N10–Pt4–Pt3 plane and N9A–N10A–Pt4–Pt3 plane, or N3–N7–Pt2–Pt1 plane and N4–N8–Pt2–Pt1 plane, are 78.1° and 74.2°, respectively, comparable to those observed in previous crown-shaped trigonal Pd6 macrocyclic structure. The dihedral angles between two pyrazolate planes in the diplatinum corners are 70.8° (Pt1Pt2 corner) and 72.9° (Pt3Pt4 corner), notably smaller than those of Pd8 macrocyclic structure. Complex **3b** crystallized in the monoclinic space group $C2/m$. Selected bond lengths and bond angles are listed in Table S5.

The dihedral angles between the bpy ligands within the dimetal corners are 90.8° (bpy)Pt3 and (bpy)Pt4) and 88.7° ((bpy)Pt1 and (bpy)Pt2), which are slightly larger than those observed for **2a**. The separations of Pt1···Pt2 and Pt3···Pt4 are 3.372(1) Å and 3.349(1) Å, respectively, which display weak Pt···Pt interactions. The side view of **3b** presents a crown conformation with the side length of the crown rims ≈ 13.7 Å and cavity depth ≈ 10.0 Å. The packing of the triangular molecules in crystals of **3b** is also interesting. In the crystal, complex **3b** stacks by weak intermolecular

$\pi \cdots \pi$ stacking interactions with a contact distance of 3.739(7) Å between two bpy rings of the neighboring molecules (Figure S23). The molecules are stacked with alternating orientations differing by about 60°. Thus, a projection along the stacking direction gives a hexagonal cross section, and the channel is filled with disordered solvent molecules.

Photophysical Studies. The electronic absorption spectra of **1** and **2** in methanol at 298 K exhibited an intense high-energy absorption band at 280–330 nm with an absorption shoulder at 340–415 nm, as shown in Figure 12. As a similar absorption pattern was observed in their corresponding precursor complexes, **C1** and **C2**, the high-energy absorption band was assigned as $\pi \rightarrow \pi^*$ intraligand (IL) transition of the bipyridyl ligand. Upon excitation at $\lambda \geq 400$ nm, the emission spectra of both **1** and **2** (concentration $\geq 1 \times 10^{-5}$ M) in methanol at 298 K showed a structureless emission band at 608 nm. A diminishment of emission intensity with I/I_0 of about 0.6 upon exposure to atmospheric oxygen, together with the observation of the large Stokes shift between the emission and excitation maxima (Figure 13), is

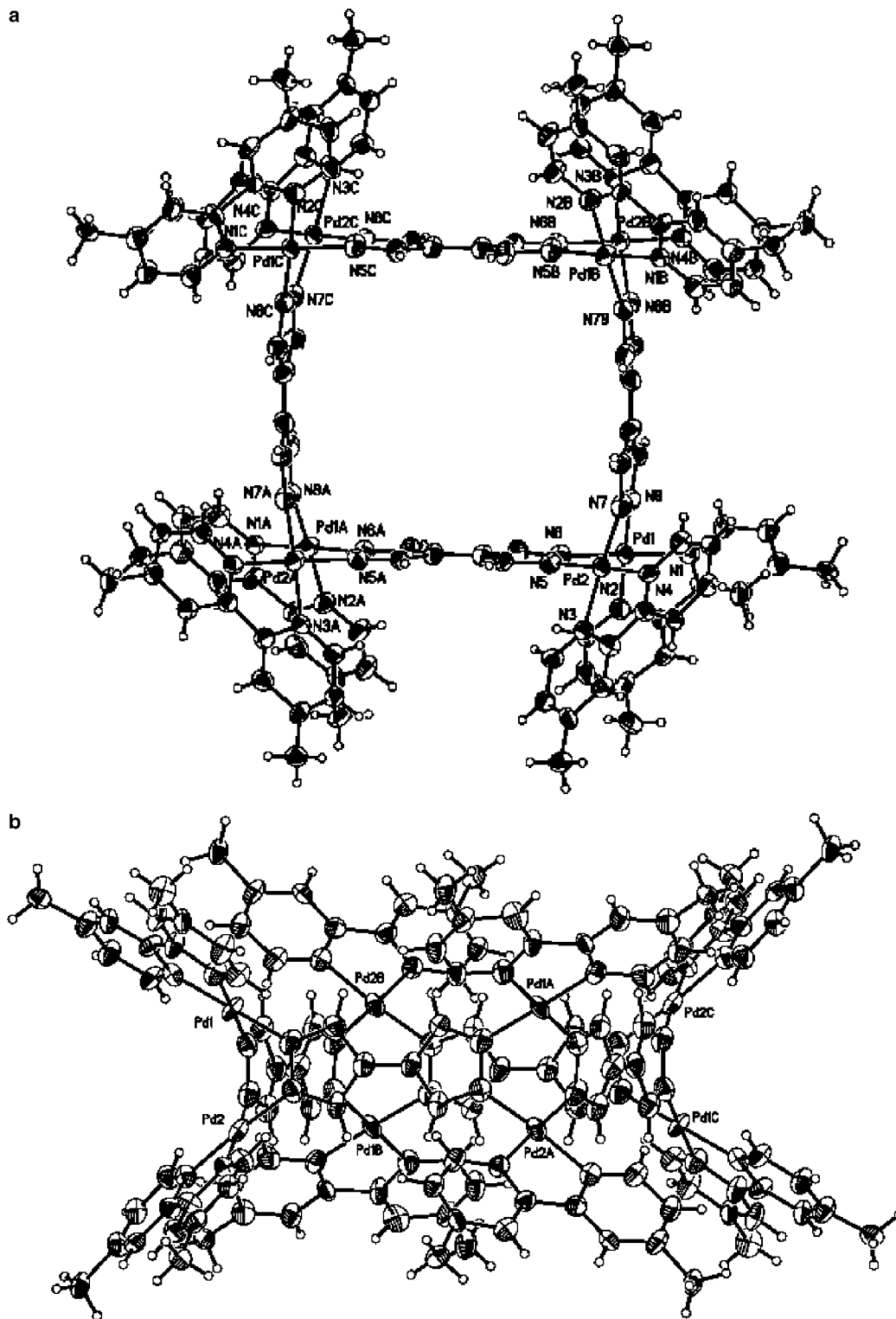


Figure 9. ORTEP diagram of **1a** showing atom-labeling scheme: (a) top view; (b) side view. Thermal ellipsoids are shown at 30% probability level. The counterions and solvent molecules are omitted for clarity.

suggestive of an emissive state of triplet parentage. An assignment of a metal-to-ligand charge transfer (MLCT) state from Pd(II) to π^* (bipyridyl) that is responsible for the emission is less likely given the instability of the Pd(III) oxidation state. Several possible assignments are suggested. In view of the short Pd \cdots Pd contact (3.345 Å) from the crystal structure of **1**, possible assignments may include triplet $d\sigma^* \rightarrow p\sigma$ metal-centered (MC) and $d\sigma^*(\text{Pd}\cdots\text{Pd})$

$\rightarrow \pi^*(\text{bipyridyl})$ metal–metal-to-ligand charge transfer (MMLCT) excited states, where $d\sigma^*$ and $p\sigma$ refer to the antibonding combination of the $4d_z$ orbital on each Pd and the bonding combination of the $5p_z$ orbital on each Pd, respectively, taking the Pd \cdots Pd axis to be the z -axis. On the other hand, triplet $p\pi(\text{bpz}) \rightarrow \pi^*(\text{bipyridyl})$ ligand-to-ligand charge transfer (LLCT) and “excimeric” intraligand excited states are also possible for the assignment of this

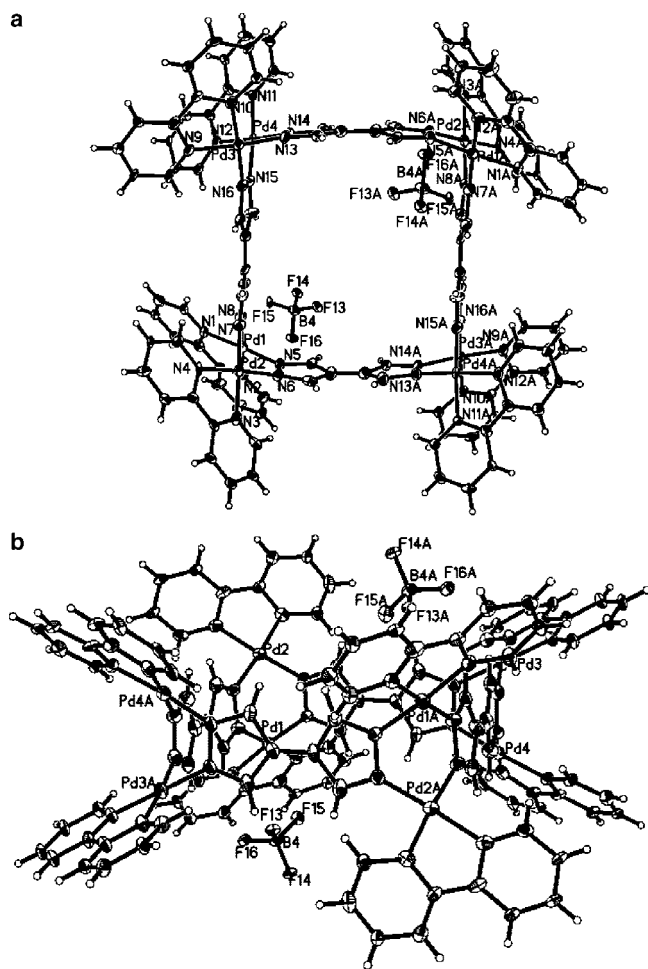


Figure 10. ORTEP diagram of **2a** showing atom-labeling scheme and two BF_4^- anions bind in the cavity: (a) top view; (b) side view. Thermal ellipsoids are shown at 30% probability level. The remaining counterions and solvent molecules are omitted for clarity.

emission band. However, since the $\text{Pd}\cdots\text{Pd}$ (2.848 Å) contact in the precursor complex **C1** is much shorter than that in **1**, the emissions of both MC and MMLCT assignments are anticipated to be lower in energy for **C1**. The observation of a higher energy emission band at 520 nm in **C1** than **1** in the same medium excludes the MC and MMLCT assignments. In view of the almost identical emission energy (620 nm) observed in **1** and **2** as well as the fact that this emission band would become more apparent with concentrations higher than 1×10^{-5} M, the emission band at 620 nm is likely due to a triplet “excimeric” intraligand excited state resulting from the intermolecular $\pi-\pi$ interaction. Such an assignment is further supported by the observation of intermolecular $\pi-\pi$ stacking (3.584 Å) interactions in the crystal packing of **1**.

Conclusions

The structures of above metallo-macrocycles show that the metal species of the dimetal clips have significant impact on the geometric architectures of the product. The dipalladium(II,II) clips tend to form $[\text{M}_8\text{L}_4]^{8+}$ -type metallo-macrocycles, while diplatinum(II,II) clips result in the mixture of $[\text{M}_8\text{L}_4]^{8+}$ and $[\text{M}_6\text{L}_3]^{6+}$ -type or other metallo-macrocycles.

Furthermore, the kinds of diimine ligands pre-coordinated with metal clips also affect the geometric architectures of the product. In the case of phen, $[\text{M}_8\text{L}_4]^{8+}$ -type metallo-macrocycles are favorable, while other ligands result in the mixture of metallo-macrocycles.

In summary, we described a series of bipyrazolate-bridged metallo-macrocycles with dipalladium(II,II) or diplatinum(II,II) clips through a spontaneous deprotonation solution self-assembly process. This approach can be extended to other polypyrazolyl ligands and other homo- or heterodimetal coordination motifs such as di-Ru, di-Rh, or Pd–Pt units, etc. Because of high stability in strong acidic aqueous solution, these nanosize cavity molecular assemblies have potential applications in such exciting fields as molecular encapsulation, molecular catalysis, and molecular reaction container.

Experimental Section

Materials. 4,4'-Dimethyl-2,2'-bipyridine (dmbpy), 2,2'-bipyridine (dmbpy), 1,10-phenanthroline (phen), potassium hexafluorophosphate (99%), and sodium tetrafluoroborate (99%) were purchased from ACROS ORGANICS and used without further purification. Methanol for photophysical experiments was of spectroscopic grade. All other chemicals and solvents were of reagent grade and were purified according to conventional methods.¹³ The bidentate ligands C5-phen,¹⁴ C6-phen,¹⁴ and C8-phen¹⁵ (Chart 1) were prepared according to literature methods. The dimetal clips **C1**–**C11** were prepared according to literature procedures.^{16,17} 4,4'-Bipyrazole (byz) was synthesized according to the published methods.¹⁸

Instrumentation. ^1H and ^{13}C NMR experiments were performed on a Bruker DMX300 and Bruker Avance DMX400 spectrometer using TMS as internal standard. ESI-MS measurements were recorded with HP5989B mass spectrometer. Elemental analyses were performed on a Thermoquest Flash EA 1112 instrument. The electronic absorption spectra were recorded on a Hewlett-Packard 8452A diode-array spectrophotometer. Steady-state emission and excitation spectra recorded at room temperature were obtained on a Spex Fluorolog-2 model F 111 fluorescence spectrophotometer with or without Corning filters.

X-ray Structural Determinations. X-ray diffraction measurements were carried out at 291 K on a Bruker Smart Apex CCD area detector equipped with a graphite monochromated Mo K α radiation ($\lambda = 0.71073$ Å). The absorption correction for all complexes was performed using SADABS. All the structures were solved by direct methods and refined employing full-matrix least-squares on F² by using SHELXTL (Bruker, 2000) program and expanded using Fourier techniques. All non-H atoms of the complexes were refined with anisotropic thermal parameters. The hydrogen atoms were included in idealized positions. Final residuals along with unit cell, space group, data collection, and refinement parameters are presented in Table 1.

- (13) Armarego, W. L. F.; Perrin, D. D. *Purification of Laboratory Chemicals*, 4th ed.; Butterworth Heinemann: Oxford, 1997.
- (14) Rice, C. R.; Guerrero, A.; Bell, Z. R.; Paul, R. L.; Motson, G. R.; Jeffery, J. C.; Ward, M. D. *New J. Chem.* **2001**, 25, 185.
- (15) Lazarides, T.; Miller, T. A.; Jeffery, J. C.; Ronson, T. K.; Adams, H.; Ward, M. D. *Dalton Trans.* **2005**, 528.
- (16) Yu, S.-Y.; Fujita, M.; Yamaguchi, K. *J. Chem. Soc., Dalton. Trans.* **2001**, 3419 and references cited therein.
- (17) Conrad, R. C.; Rund, J. V. *Inorg. Chem.* **1972**, 11, 129.
- (18) (a) Boldog, I.; Sieler, J.; Chernega, A. N.; Domasevitch, K. V. *Inorg. Chim. Acta* **2002**, 338, 69. (b) Boldog, I.; Rusanov, E. B.; Chernega, A. N.; Sieler, J.; Domasevitch, K. V. *Angew. Chem., Int. Ed.* **2001**, 40, 3435.

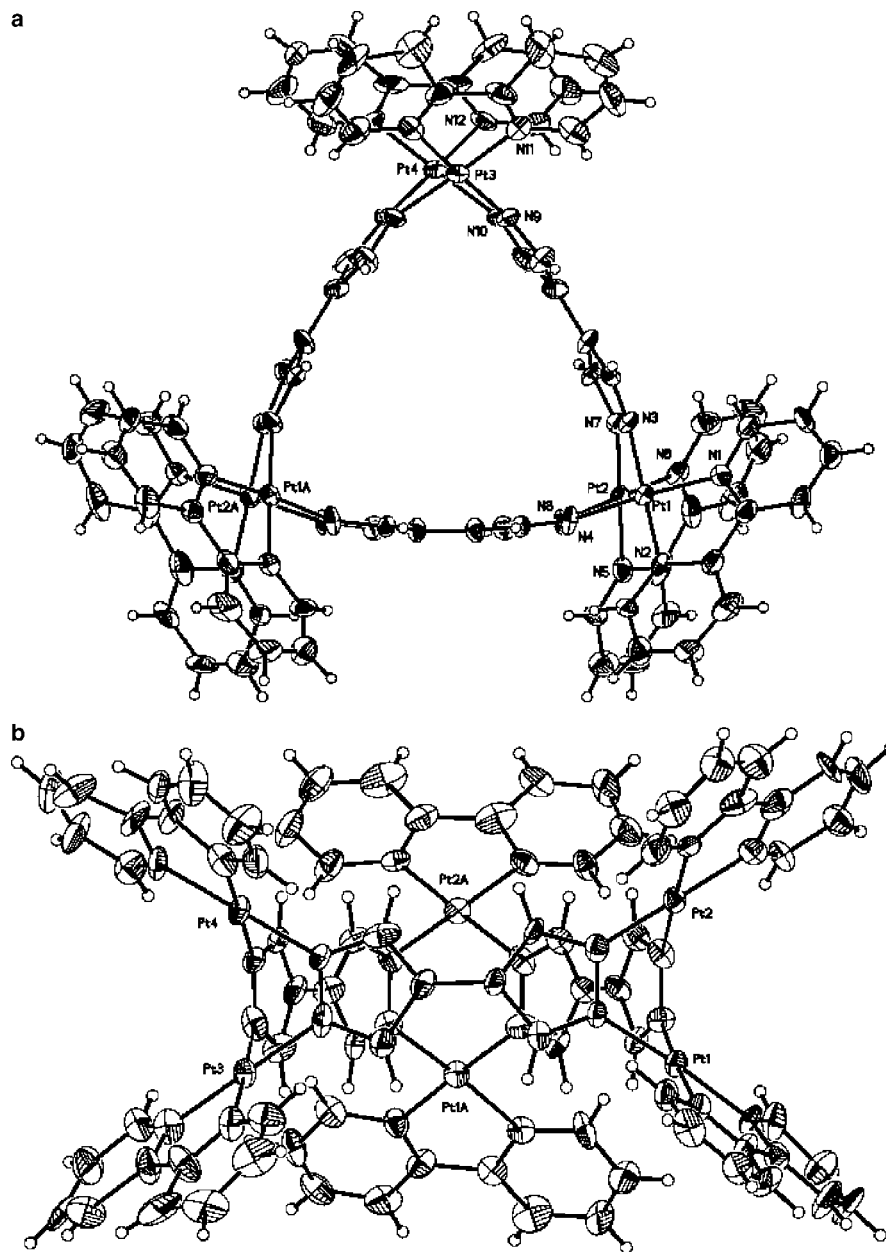


Figure 11. ORTEP diagram of **3b** showing atom-labeling scheme and the asymmetric subunit: (a) top view; (b) side view. Thermal ellipsoids are shown at 30% probability level. The counterions and solvent molecules are omitted for clarity.

Synthesis. 4,4'-Bipyrazole (bpz). Mp: >300 °C. ^1H NMR (300 MHz, $[\text{D}_6]\text{DMSO}$, 25 °C, TMS, ppm): 12.75 (s, 2H, NH); 7.87 (s, 2H, $\text{H}_{3,3'}$); 7.70 (s, 2H, $\text{H}_{5,5'}$). Anal. calcd for $\text{C}_6\text{H}_6\text{N}_4$ (%): C 53.72; H 4.51; N 41.77. Found: C 53.80; H 4.52; N 41.68.

$[\text{Pd}_8(\text{dmbpy})_8\text{L}_4](\text{NO}_3)_8$ (**1**). **C1** (83.0 mg, 0.1 mmol) was added to a suspension of bpz (13.4 mg, 0.1 mmol) in H_2O (10 mL), and the mixture was stirred for 2 h at room temperature. The resulting clear yellow solution was evaporated to dryness to give a yellow solid. Pure **1** as a microcrystalline yellow solid was obtained by the vapor diffusion of diethyl ether into a 2 mM solution of **1** in methanol at room temperature. Yield: 82.8 mg (99%). ^1H NMR (400 MHz, acetone- $d_6/\text{D}_2\text{O} = 2:1$, 25 °C, TMS, ppm): 8.53 (s, 16 H, $\text{bpy-H}_{3,3'}$), 8.35 (d, $J = 5.9$ Hz, 16 H, $\text{bpy-H}_{6,6'}$), 8.25 (s, 16H, $\text{bpz-H}_{3,5,3',5'}$), 7.75 (d, $J = 5.6$ Hz, 8H, $\text{bpy-H}_{5,5'}$), 2.70 (s, 24H, dmbpy-CH_3). ^{13}C NMR (100.6 MHz, acetone- $d_6/\text{D}_2\text{O} = 2:1$, 25 °C, TMS, ppm): 155.7, 155.6, 150.0, 137.1, 128.7, 124.7, 116.7, 20.8 (CH_3). UV/vis (methanol, ϵ , $\text{M}^{-1}\text{cm}^{-1}$): $\lambda_{\text{max}} = 210$ (478 680), 240 (307 600), 304 (106 800), 314 (sh, 95 270), 392 nm (sh,

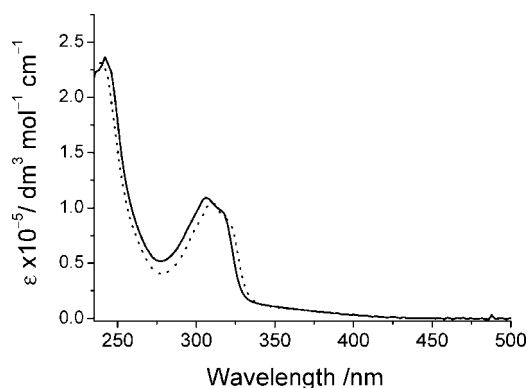


Figure 12. Electronic absorption spectra of **1** (—) and **2** (---) in methanol at 298 K.

20 830). Emission (methanol): $\lambda_{\text{max}} = 442$ nm. Elem anal. calcd for $\text{C}_{120}\text{H}_{112}\text{N}_{40}\text{O}_{24}\text{Pd}_8 \cdot 4\text{H}_2\text{O}$ (%): C 42.12; H 3.53; N 16.37; found:

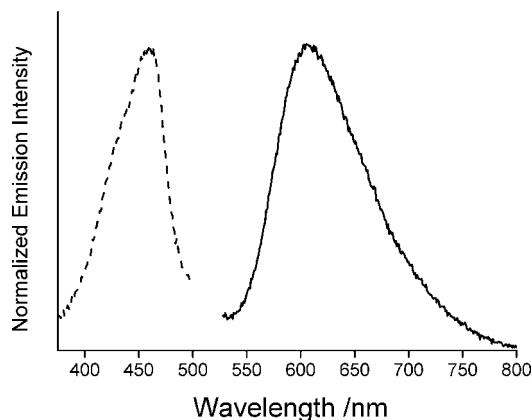


Figure 13. Emission (—) and excitation (---) spectra of **1** (concentration = 1×10^{-5} M) in methanol at 298 K.

C 42.05; H 3.83; N 16.01. ESI-MS (methanol): m/z 1054.4 [**1** – 3NO_3^-] $^{3+}$, 775.3 [**1** – 4NO_3^-] $^{4+}$, 607.8 [**1** – 5NO_3^-] $^{5+}$, 496.3 [**1** – 6NO_3^-] $^{6+}$.

The BF_4^- salt of **1** (**1a**) was obtained by adding a 10-fold excess of NaBF_4 to its aqueous solution at 333 K, which resulted in the immediate deposition of **1a** as yellow microcrystals in quantitative yield. The crystals were filtered, washed with minimum amount of cold water, and dried under vacuum. ^1H NMR (400 MHz, CD_3CN , 25 °C, ppm): 8.25 (s, 16 H, bpy- $\text{H}_{3,3'}$), 8.06 (d, $J = 5.9$ Hz, 16 H, bpy- $\text{H}_{6,6'}$), 7.93 (s, 16H, bpz- $\text{H}_{3,5,3',5'}$), 7.54 (d, $J = 5.6$ Hz, 8H, bpy- $\text{H}_{5,5'}$), 2.60 (s, 24H, dmbpy- CH_3). ESI-MS (acetonitrile): m/z 1095.7 [**1a** – 3BF_4^-] $^{3+}$, 800.1 [**1a** – 4BF_4^-] $^{4+}$, 622.8 [**1a** – 5BF_4^-] $^{5+}$, 504.5 [**1a** – 6BF_4^-] $^{6+}$, 420.0 [**1a** – 7BF_4^-] $^{7+}$, 356.7 [**1a** – 8BF_4^-] $^{8+}$. Elem anal. calcd for $\text{C}_{120}\text{H}_{112}\text{N}_{32}\text{B}_8\text{F}_{32}\text{Pd}_8 \cdot 10\text{H}_2\text{O}$ (%): C 38.66; H 3.57; N 12.02; found: C 38.65; H 3.46; N 12.01. X-ray quality crystals were grown by the vapor diffusion of diethyl ether into a 1.0 mM solution of **1a** in acetonitrile at room temperature.

[$\text{Pd}_8(\text{bpy})_8\text{L}_4](\text{NO}_3)_8$ (**2**). The same procedure as employed for **1** was followed except that **C2** (77.2 mg, 0.1 mmol) and bpz (13.4 mg, 0.1 mmol) were used as the starting materials. Pure **2** as a microcrystalline yellow solid was obtained by the vapor diffusion of diethyl ether into a 2 mM solution of **2** in methanol at room temperature. Yield: 74.4 mg (97.8%). ^1H NMR (400 MHz, acetone- $d_6/\text{D}_2\text{O} = 2:1$, 25 °C, TMS, ppm): 8.65 (d, $J = 8.1$ Hz, 16 H; bpy- $\text{H}_{6,6'}$), 8.50 (m, 32H; bpy- $\text{H}_{3,3'}$ and bpy- $\text{H}_{5,5'}$), 8.28 (s, 16H; bpz- $\text{H}_{3,5,3',5'}$), 7.90 (t, $J = 6.5$ Hz, 16H; bpy- $\text{H}_{4,4'}$). ^{13}C NMR (75.5 MHz, acetone- $d_6/\text{D}_2\text{O} = 2:1$, 25 °C, TMS, ppm): 154.8, 149.5, 141.2, 135.8, 126.9, 122.8, 115.3 ppm. UV/vis (methanol, ϵ , $\text{M}^{-1} \text{cm}^{-1}$): $\lambda_{\text{max}} = 204$ (456 660), 238 (255 330), 308 (103 500), 317 (sh, 88 190), 392 nm (sh, 20 830). Emission (methanol): $\lambda_{\text{max}} = 440$ nm. Elem anal. calcd for $\text{C}_{104}\text{H}_{80}\text{N}_{40}\text{O}_{24}\text{Pd}_8 \cdot 16\text{H}_2\text{O}$ (%): C 36.59, H 3.30, N 16.41; found: C 36.31, H 3.13, N 16.35. ESI-MS (methanol): m/z 979.6 [**2** – 3NO_3^-] $^{3+}$, 719.5 [**2** – 4NO_3^-] $^{4+}$, 563.7 [**2** – 5NO_3^-] $^{5+}$, 459.0 [**2** – 6NO_3^-] $^{6+}$, 384.6 [**2** – 7NO_3^-] $^{7+}$, 328.4 [**2** – 8NO_3^-] $^{8+}$.

The BF_4^- salt of **2** (**2a**) was obtained by adding a 10-fold excess of NaBF_4 to its aqueous solution at 333 K, which resulted in the immediate deposition of **2a** as yellow microcrystals in quantitative yield. The crystals were filtered, washed with minimum amount of cold water, and dried under vacuum. ^1H NMR (400 MHz, CD_3CN , 25 °C, ppm): 8.44 (d, $J = 8.0$ Hz, 16 H; bpy- $\text{H}_{6,6'}$), 8.36 (t, $J = 7.7$ Hz, 16H; bpy- $\text{H}_{5,5'}$), 8.25 (d, $J = 5.4$ Hz, 16H; bpy- $\text{H}_{3,3'}$), 7.98 (s, 16H; bpz- $\text{H}_{3,5,3',5'}$), 7.72 (t, $J = 6.6$ Hz, 16H; bpy- $\text{H}_{4,4'}$). Elem anal. calcd for $\text{C}_{104}\text{H}_{80}\text{N}_{32}\text{B}_8\text{F}_{32}\text{Pd}_8 \cdot 10\text{H}_2\text{O}$ (%): C 35.64, H 2.88, N

12.79; found: C 35.53, H 2.77, N 12.82. X-ray quality crystals were grown by the vapor diffusion of diethyl ether into a 1.0 mM solution of **2a** in acetonitrile at room temperature.

[$\text{Pt}_8(\text{bpy})_8\text{L}_4](\text{NO}_3)_8$ (**3a**) and [$\text{Pt}_6(\text{bpy})_6\text{L}_3](\text{NO}_3)_6$ (**3b**). **C3** (96.0 mg, 0.1 mmol) was added to a suspension of bpz (13.4 mg, 0.1 mmol) in H_2O (10 mL), and the mixture was stirred for 24 h at 90 °C. The resulting clear yellow solution was evaporated to dryness to give a yellow solid. This was identified by NMR spectroscopy as a mixture of **3a** and **3b** (50:50). All attempts to separate the mixture by repeated recrystallizations were unsuccessful due to the similar solubility of the compounds. Yield: 382.0 mg (97.8%). ^1H NMR (400 MHz, acetone- $d_6/\text{D}_2\text{O} = 2:1$, 25 °C, TMS, ppm): 8.90 (m, bpy- $\text{H}_{6,6'}$), 8.76 (m, bpy- $\text{H}_{3,3'}$), 8.65 (m, bpy- $\text{H}_{5,5'}$), 8.44 (s, bpz- $\text{H}_{3,5,3',5'}$, **3a**), 8.40 (s, bpz- $\text{H}_{3,5,3',5'}$, **3b**), 8.02 (m, bpy- $\text{H}_{4,4'}$). ESI-MS (methanol): m/z 896.9 [**3a** – 4NO_3^-] $^{4+}$ and [**3b** – 3NO_3^-] $^{3+}$, 704.9 [**3a** – 5NO_3^-] $^{5+}$, 656.8 [**3b** – 4NO_3^-] $^{4+}$, 577.1 [**3a** – 6NO_3^-] $^{6+}$, 513.2 [**3b** – 5NO_3^-] $^{5+}$.

[$\text{Pd}_8(\text{phen})_8\text{L}_4](\text{NO}_3)_8$ (**4**). The same procedure as employed for **1** was followed except that **C4** (82.2 mg, 0.1 mmol) and bpz (13.4 mg, 0.1 mmol) were used as the starting materials. Yield: 82.0 mg (99%). ^1H NMR (300 MHz, $\text{DMSO}-d_6$, 25 °C, TMS, ppm): 9.07 (d, $J = 8.1$ Hz, 16 H; phen- $\text{H}_{2,9}$), 8.78 (d, $J = 4.9$ Hz, 16 H; phen- $\text{H}_{4,7}$), 8.47 (s, 16H; bpz- $\text{H}_{3,5,3',5'}$), 8.36 (s, 16H; phen- $\text{H}_{5,6}$), 8.19 (dd, $J_1 = 7.9$, $J_2 = 5.6$ Hz, 16H; phen- $\text{H}_{3,8}$). Elem anal. calcd for $\text{C}_{120}\text{H}_{80}\text{N}_{40}\text{O}_{24}\text{Pd}_8 \cdot 6\text{H}_2\text{O}$ (%): C 42.07, H 2.71, N 16.36; found: C 41.96, H 2.76, N 16.21.

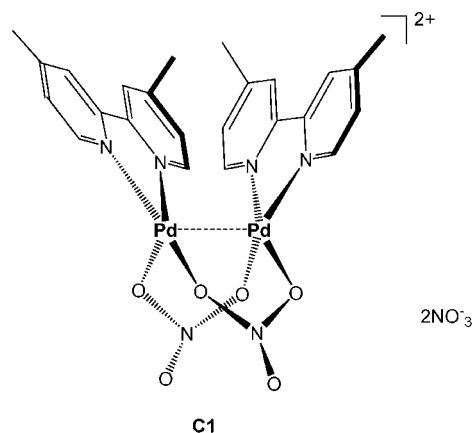
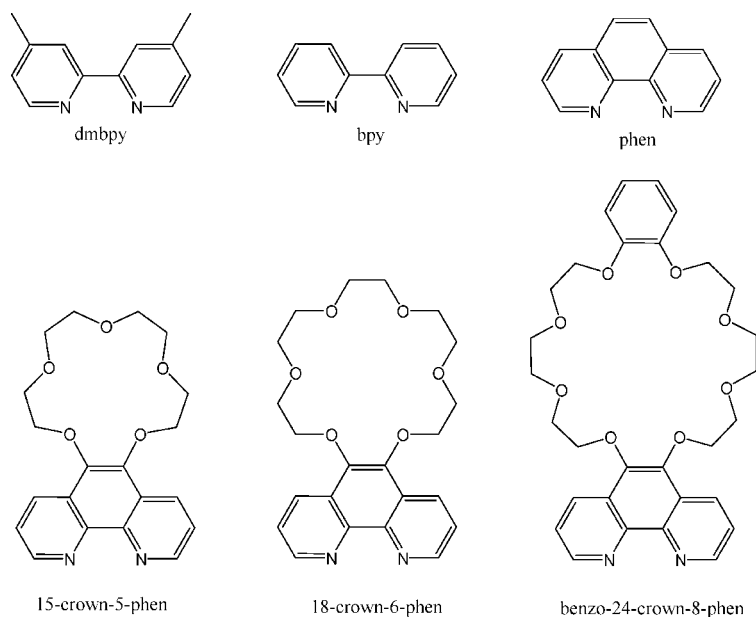
The PF_6^- salt of **4** (**4a**) was prepared by exchange with a 10-fold excess of KPF_6 in aqueous solution. ^1H NMR (400 MHz, CD_3CN , 25 °C, ppm): 8.95 (d, $J = 8.3$ Hz, 16 H; phen- $\text{H}_{2,9}$), 8.74 (d, $J = 5.2$ Hz, 16 H; phen- $\text{H}_{4,7}$), 8.27 (s, 16H; bpz- $\text{H}_{3,5,3',5'}$), 8.22 (s, 16H; phen- $\text{H}_{5,6}$), 8.09 (dd, $J_1 = 8.3$, $J_2 = 5.4$ Hz, 16H; phen- $\text{H}_{3,8}$). ESI-MS (CH_3CN): m/z 1181.9 [**4a** – 3PF_6^-] $^{3+}$, 850.4 [**4a** – 4PF_6^-] $^{4+}$, 651.0 [**4a** – 5PF_6^-] $^{5+}$, 581.5 [**4a** – 6PF_6^-] $^{6+}$, 424.0 [**4a** – 7PF_6^-] $^{7+}$, 352.6 [**4a** – 8PF_6^-] $^{8+}$. Elem anal. calcd for $\text{C}_{120}\text{H}_{80}\text{N}_{32}\text{F}_{48}\text{P}_8\text{Pd}_8 \cdot 6\text{H}_2\text{O}$ (%): C 35.25, H 2.27, N 10.96; found: C 35.12, H 2.32, N 10.85.

[$\text{Pt}_8(\text{phen})_8\text{L}_4](\text{NO}_3)_8$ (**5**). The same procedure as employed for **2** was followed except that **C5** (99.9 mg, 0.1 mmol) and bpz (13.4 mg, 0.1 mmol) were used as the starting materials. Yield: 97.7 mg (97%). The PF_6^- salt of **5** (**5a**) was prepared by exchange with a 10-fold excess of KPF_6 in aqueous solution. ^1H NMR (400 MHz, CD_3CN , 25 °C, ppm): 9.14 (d, $J = 4.8$ Hz, 16 H; phen- $\text{H}_{4,7}$), 9.00 (d, $J = 8.3$ Hz, 16 H; phen- $\text{H}_{2,9}$), 8.41 (s, 16H; bpz- $\text{H}_{3,5,3',5'}$), 8.29 (s, 16H; phen- $\text{H}_{5,6}$), 8.21 (dd, $J_1 = 8.3$, $J_2 = 5.5$ Hz, 16H; phen- $\text{H}_{3,8}$). Elem anal. calcd for $\text{C}_{120}\text{H}_{80}\text{N}_{40}\text{O}_{24}\text{Pt}_8 \cdot 12\text{H}_2\text{O}$ (%): C 33.97, H 2.47, N 13.20; found: C 33.89, H 2.36, N 13.12.

[$\text{Pd}_8(\text{C5-phen})_8\text{L}_4](\text{NO}_3)_8$ (**6**). The same procedure as employed for **1** was followed except that **C6** (120.2 mg, 0.1 mmol) and bpz (13.4 mg, 0.1 mmol) were used as the starting materials. Yield: 119.8 mg (99%). ^1H NMR (400 MHz, acetone- $d_6/\text{D}_2\text{O} = 2:1$, 25 °C, TMS, ppm): 9.23 (d, $J = 8.4$ Hz, 16 H; phen- $\text{H}_{2,9}$), 8.98 (d, $J = 4.9$ Hz, 16 H; phen- $\text{H}_{4,7}$), 8.54 (s, 16H; bpz- $\text{H}_{3,5,3',5'}$), 8.29 (dd, $J_1 = 8.1$, $J_2 = 5.4$ Hz, 16H; phen- $\text{H}_{3,8}$), 4.65 (m, 32H; OCH_2), 4.21 (m, 32H; CH_2O), 3.94 (m, 32H; OCH_2), 3.90 (m, 32H; CH_2O). Elem anal. calcd for $\text{C}_{184}\text{H}_{192}\text{N}_{40}\text{O}_{64}\text{Pd}_8 \cdot 18\text{H}_2\text{O}$ (%): C 42.80, H 4.45, N 10.85; found: C 42.79, H 4.57, N 10.71.

The PF_6^- salt of **6** (**6a**) was prepared by exchange with a 10-fold excess of KPF_6 in aqueous solution. ^1H NMR (400 MHz, CD_3CN , 25 °C, ppm): 9.02 (d, $J = 8.5$ Hz, 16 H; phen- $\text{H}_{2,9}$), 8.60 (d, $J = 5.2$ Hz, 16 H; phen- $\text{H}_{4,7}$), 8.17 (s, 16H; bpz- $\text{H}_{3,5,3',5'}$), 8.01 (dd, $J_1 = 8.4$, $J_2 = 5.4$ Hz, 16H; phen- $\text{H}_{3,8}$), 4.47 (m, 32H; OCH_2), 4.01 (m, 32H; CH_2O), 3.72 (m, 32H; OCH_2), 3.65 (m, 32H; CH_2O). Elem anal. calcd for $\text{C}_{184}\text{H}_{192}\text{F}_{48}\text{N}_{32}\text{O}_{40}\text{P}_8\text{Pd}_8 \cdot 12\text{H}_2\text{O}$ (%): C 38.64,

Chart 1



- C1** = [Pd(dmbpy)]₂(NO₃)₂
C2 = [Pd(bpy)]₂(NO₃)₂
C3 = [Pt(bpy)]₂(NO₃)₂
C4 = [Pd(phen)]₂(NO₃)₂
C5 = [Pt(phen)]₂(NO₃)₂
C6 = [Pd(15-Crown-5-phen)]₂(NO₃)₂
C7 = [Pt(15-Crown-5-phen)]₂(NO₃)₂
C8 = [Pd(18-Crown-6-phen)]₂(NO₃)₂
C9 = [Pt(18-Crown-6-phen)]₂(NO₃)₂
C10 = [Pd(benzo-24-Crown-8-phen)]₂(NO₃)₂
C11 = [Pt(benzo-24-Crown-8-phen)]₂(NO₃)₂

H 3.81, N 7.84; found: C 38.56, H 3.79, N 7.80. ESI-MS (CH₃CN): *m/z* 1689.1 [6a - 3PF₆]³⁺, 1230.6 [6a - 4PF₆]⁴⁺, 955.7 [6a - 5PF₆]⁵⁺, 772.3 [6a - 6PF₆]⁶⁺, 641.2 [6a - 7PF₆]⁷⁺.

[Pt₈(C5-phen)₈L₄](NO₃)₈ (**7a**), [Pt₆(C5-phen)₆L₃](NO₃)₆ (**7b**), and Other Macrocycle (**7c**). The same procedure as employed for **2** was followed except that **C7** (137.9 mg, 0.1 mmol) and bpz (13.4 mg, 0.1 mmol) were used as the starting materials, which afforded the mixture of **7a**, **7b**, and **7c** (65:24:11) as a yellow solid. Yield: 135.8 mg (98%). ¹H NMR (400 MHz, acetone-*d*₆/D₂O = 2:1, 25 °C, TMS, ppm): 9.30–9.10 (m, phen-H_{24,7,9}), 8.64 (s, bpz-H_{3,5,3',5'}, **7c**), 8.59 (s, bpz-H_{3,5,3',5'}, **7a**), 8.52 (s, bpz-H_{3,5,3',5'}, **7b**), 8.34 (m, phen-H_{3,8}, **7c**), 8.30 (m, phen-H_{3,8}, **7a**), 8.24 (m, phen-H_{3,8}, **7b**), 4.61 (m, OCH₂), 4.13 (m, CH₂O), 3.85 (m, OCH₂), 3.80 (m, CH₂O).

[Pd₈(C6-phen)₈L₄](NO₃)₈ (**8**). The same procedure as employed for **1** was followed except that **C8** (129.0 mg, 0.1 mmol) and bpz (13.4 mg, 0.1 mmol) were used as the starting materials. Yield: 127.2 mg (98%). ¹H NMR (400 MHz, acetone-*d*₆/D₂O = 2:1, 25 °C, TMS, ppm): 9.19 (d, *J* = 8.5 Hz, 16 H; phen-H_{2,9}), 8.94 (d, *J* = 4.9 Hz, 16 H; phen-H_{4,7}), 8.49 (s, 16H; bpz-H_{3,5,3',5'}), 8.25 (dd, *J*₁ = 7.9, *J*₂ = 5.6 Hz, 16H; phen-H_{3,8}), 4.62 (m, 32H; OCH₂), 4.10 (m, 32H; CH₂O), 3.84 (m, 32H; OCH₂), 3.81 (m, 32H; CH₂O), 3.75 (s, 32H; OCH₂CH₂O). Elem anal. calcd for

C₂₀₀H₂₂₄N₄₀O₇₂Pd₈·23H₂O (%): C 42.85, H 4.85, N 9.99; found: C 42.94, H 4.80, N 9.86. ESI-MS (methanol): *m/z* 1236.2 [8 - 4NO₃]⁴⁺, 976.4 [8 - 5NO₃]⁵⁺.

The PF₆⁻ salt of **8** (**8a**) was prepared by exchange with a 10-fold excess of KPF₆ in aqueous solution. ¹H NMR (400 MHz, CD₃CN, 25 °C, ppm): 9.04 (d, *J* = 8.5 Hz, 16 H; phen-H_{2,9}), 8.64 (d, *J* = 5.2 Hz, 16 H; phen-H_{4,7}), 8.20 (s, 16H; bpz-H_{3,5,3',5'}), 8.05 (dd, *J*₁ = 8.4, *J*₂ = 5.4 Hz, 16H; phen-H_{3,8}), 4.51 (m, 32H; OCH₂), 3.96 (m, 32H; CH₂O), 3.71 (m, 32H; OCH₂), 3.68 (m, 32H; CH₂O), 3.64 (s, 32H; OCH₂CH₂O). Elem anal. calcd for C₂₀₀H₂₂₄N₃₂O₄₈F₄₈P₈Pd₈·15H₂O (%): C 39.22, H 4.18, N 7.32; found: C 39.21, H 4.30, N 7.22.

[Pt₈(C6-phen)₈L₄](NO₃)₈ (**9a**) and [Pt₆(C6-phen)₆L₃](NO₃)₆ (**9b**). The same procedure as employed for **2** was followed except that **C9** (146.7 mg, 0.1 mmol) and bpz (13.4 mg, 0.1 mmol) were used as the starting materials. Yield: 144.7 mg (98%). This was identified by NMR spectroscopy as a mixture of **9a** and **9b** (50:50). The pure compounds of **9a** and **9b** also can not be isolated by repeated recrystallizations due to their similar solubility. ¹H NMR (400 MHz, acetone-*d*₆/D₂O = 2:1, 25 °C, TMS, ppm): 9.40–9.23 (m, phen-H_{2,9} and phen-H_{4,7}, **9a** and **9b**), 8.65 (s, bpz-H_{3,5,3',5'}, **9a**), 8.57 (s, bpz-H_{3,5,3',5'}, **9b**), 8.35 (dd, *J*₁ = 8.2, *J*₂ = 5.3 Hz, phen-

Table 1. Crystallographic Data for Complexes **1a**, **2a**, and **3b**

	1a ·26H ₂ O	2a ·14H ₂ O	3b ·12H ₂ O
empirical formula	C ₁₂₀ H ₁₆₄ B ₈ F ₃₂ N ₃₂ O ₂₆ Pd ₈	C ₁₀₄ H ₁₀₈ B ₈ F ₃₂ N ₃₂ O ₁₄ Pd ₈	C ₇₈ H ₈₄ N ₃₀ O ₃₀ Pt ₆
fw	4016.51	3575.90	3092.24
cryst syst, space group	monoclinic, C2/m	triclinic, P $\bar{1}$	monoclinic, C2/m
<i>a</i> , Å	25.615(5)	13.973(3)	25.7736(12)
<i>b</i> , Å	33.112(7)	16.063(3)	29.8901(13)
<i>c</i> , Å	17.229(3)	19.451(4)	19.4796(12)
α , deg	90.00	111.18(3)	90.00
β , deg	128.04(3)	100.82(3)	120.374(15)
γ , deg	90.00	91.69(3)	90.00
<i>V</i> , Å ³	11509(6)	3975.8(17)	12947(2)
<i>Z</i>	2	1	4
ρ_{calcd} , g cm ⁻³	1.159	1.494	1.586
μ , mm ⁻¹	0.673	0.979	6.529
<i>F</i> (000)	4024	1764	5880
transm range	0.820–0.875	0.74–0.78	0.15–0.21
θ range, deg	1.20–26.00	1.15–26.00	1.14–26.00
no. data	11535	15619	24092
no. params	619	970	713
GOF ^a	0.997	1.074	1.017
R1, wR2 [<i>I</i> > 2 σ (<i>I</i>)] ^b	0.0554, 0.0901	0.0566, 0.1106	0.0654, 0.1488
R1, wR2 (all data) ^b	0.0922, 0.0952	0.07690, 0.1145	0.1141, 0.1488

^a GOF = $\{\sum[w(F_o^2 - F_c^2)^2]/(n - p)\}^{1/2}$, where *n* and *p* denote the number of data points and the number of parameters, respectively. ^b R1 = $(\sum||F_o| - |F_c||)/\sum|F_o|$; wR2 = $\{\sum[[w(F_o^2 - F_c^2)^2]/\sum w(F_o^2)^2]\}^{1/2}$, where $w = 1/[\delta^2(F_o^2) + (aP)^2 + bP]$ and $P = [\max(0, F_o^2) + 2F_c^2]/3$.

H_{3,8}, **9a**), 8.29 (dd, *J*₁ = 8.2, *J*₂ = 5.3 Hz, phen-H_{3,8}, **9b**), 4.70 (m, OCH₂), 4.23 (m, CH₂O), 3.95 (m, OCH₂CH₂O).

[Pd₈(C8-phen)₈L₄](NO₃)₈ (10a) and [Pd₆(C8-phen)₆L₃](NO₃)₈ (10b). The same procedure as employed for **1** was followed except that **C10** (146.6 mg, 0.1 mmol) and bpz (13.4 mg, 0.1 mmol) were used as the starting materials. Yield: 142.5 mg (97%). The BF₄⁻ salt of **10** (**10a**) was obtained by adding a 10-fold excess of NaBF₄ to its aqueous solution at 333 K, which resulted in the immediate deposition of **10a** as yellow microcrystals in quantitative yield. The crystals were filtered, washed with minimum amount of cold water, and dried under vacuum, which afforded the mixture of **10a** and **10b** (65:35) as a yellow solid. All attempts to separate the mixture by repeated recrystallizations were unsuccessful due to the similar solubility of the compounds. ¹H NMR (400 MHz, CD₃CN, 25 °C, ppm): 9.07 (m, phen-H_{2,9}), 8.60 (m, phen-H_{4,7}), 8.24 (s, bpz-H_{3,5,3',5'}, **10a**), 8.20 (s, bpz-H_{3,5,3',5'}, **10b**), 7.98 (dd, *J*₁ = 8.3, *J*₂ = 5.3 Hz, phen-H_{3,8}, **10a**), 7.95 (dd, *J*₁ = 8.3, *J*₂ = 5.3 Hz, phen-H_{3,8}, **10b**), 6.84 (m, Ph-H), 6.78 (m, Ph-H), 4.49 (m, OCH₂), 4.09 (m, CH₂O), 3.96 (m, OCH₂), 3.81 (m, OCH₂), 3.70 (s, OCH₂CH₂O), 3.62 (s, OCH₂CH₂O).

[Pt₈(C8-phen)₈L₄](NO₃)₈ (11a) and [Pt₆(C8-phen)₆L₃](NO₃)₈ (11b). The same procedure as employed for **2** was followed except that **C11** (164.3.0 mg, 0.1 mmol) and bpz (13.4 mg, 0.1 mmol)

were used as the starting materials. Yield: 162.2 mg (98%). This was identified by NMR spectroscopy as a mixture of **11a** and **11b** (85:15). All attempts to separate the mixture by repeated recrystallizations were unsuccessful due to the similar solubility of the compounds. ¹H NMR (400 MHz, acetone-*d*₆/D₂O = 2:1, 25 °C, TMS, ppm): 9.21 (m, phen-H_{2,9}), 9.13 (m, phen-H_{4,7}, **11a**), 8.97 (m, phen-H_{4,7}, **11b**), 8.57 (s, bpz-H_{3,5,3',5'}, **11a**), 8.50 (s, bpz-H_{3,5,3',5'}, **11b**), 8.16 (m, phen-H_{3,8}, **11a**), 8.10 (m, phen-H_{3,8}, **11b**), 6.62 (m, Ph-H), 6.41 (m, Ph-H), 4.59 (m, OCH₂), 4.02 (m, CH₂O), 3.87–3.74 (m, OCH₂CH₂O).

Acknowledgment. This project was supported by National Natural Science Foundation of China (No. 50673098 and 20772152).

Supporting Information Available: ¹H NMR spectra of **1–11**; ESI-MS spectra of **1, 2, 4, 7, 8, 9, 10, 11**, and **12**; tables of selected bond lengths and bond angles for **1a, 2a**, and **3b**; packing diagrams of **1a, 2a**, and **3b**; X-ray crystallographic files, in CIF format, for complexes **1a, 2a**, and **3b**. These materials are available free of charge via the Internet at <http://pub.acs.org>.

IC701344P